Wind and Structures, *Vol. 17, No. 1(2013) 043-068*
DOI:http://dx.doi.org/10.12989/was.2013.17.1.043

Statistical characteristics of sustained wind environment for a long-span bridge based on long-term field measurement data

Youliang Ding*, Guangdong Zhou, Aiqun Li and Yang Deng

Key Laboratory of Concrete and Prestressed Concrete Structures of Ministry of Education, Southeast University, Nanjing, 210096, China

(Received November 16, 2010, Revised May 8, 2012, Accepted October 3, 2012)

Abstract. The fluctuating wind induced vibration is one of the most important factors which has been taken into account in the design of long-span bridge due to the low stiffness and low natural frequency. Field measurement characteristics of sustained wind on structure site can provide accurate wind load parameters for wind field simulation and structural wind resistance design. As a suspension bridge with 1490 m main span, the Runyang Suspension Bridge (RSB) has high sensitivity to fluctuating wind. The simultaneous and continuously wind environment field measurement both in mid-span and on tower top is executed from 2005 up to now by the structural health monitoring system installed on this bridge. Based on the recorded data, the wind characteristic parameters, including mean wind speed, wind direction, the turbulence intensity, the gust factors, the turbulence integral length, power spectrum and spatial correlation, are analyzed in detail and the coherence functions of those parameters are evaluated using statistical method in this paper. The results indicate that, the turbulence component of sustain wind is larger than extremely strong winds although its mean wind speed is smaller; the correlation between turbulence parameters is obvious; the power spectrum is special and not accord with the Simiu spectrum and von Karman spectrum. Results obtained in this study can be used to evaluate the long term reliability of the Runyang Suspension Bridge and provide reference values for wind resistant design of other structures in this region.

Keywords: long-span bridge; structural health monitoring; wind environment; field measurement; turbulence characteristics; power spectrum

1. Introduction

Long-span bridges were constructed one after another in order to meet the needs of modern society for advanced transportation systems. Modern bridges are usually constructed with innovative structural systems and high strength materials; tend to be more flexible and low damping than those in the past. As a consequence, the sensitivity of these bridges to dynamic excitations, such as fluctuating wind, has increased (Liu *et al*. 2009). Zhang (2011) investigated the wind-induced instability of a long-span suspension bridge with different 3D cable systems. Nature wind has become a predominating load factor for bridge design. Therefore, the clearly understanding the wind turbulent characteristics and the prediction of wind-induced structural response is an important task.

*Corresponding author, Professor, E-mail: civilding@yahoo.com.cn

http://www.techno-press.org/?journal=was&subpage=8 ISSN: 1226-6116 (Print), 1598-6225 (Online)

The wind turbulent characteristics in the near-ground atmospheric boundary layer always display severely random fluctuation and influenced by the geography of the surface of the earth. This randomness is presented as complex turbulence in a certain time and random variation in the corresponding wind characteristic parameters (Panofsky and Dutton 1984). Investigation on wind turbulent characteristics in different places is very necessary for local structural wind resistance design. During the last few decades, wind characteristics databases have been established according to different places in some countries, such as the Sparks database of the USA (Sparks *et al*. 1992), the Kato and Ohukuma database in the Japan (Kato *et al*. 1992), the Froya database in the Norway (Andersen and Lovseth 1995), and the BWEA database in the UK (BWEA 2008). But most of those databases are for meteorological purposes. Furthermore, those databases can not be applied in other places with different geographic environment. Therefore, some actual field wind characteristics measurements special for long-span bridges have been conducted. Brownjohn *et al.* (1994) investigated the wind characteristics of Humber Bridge through long-term full-scale measurement campaigns from 1990 to 1991 to validate mathematical modeling of the response of long span bridge to wind. For the limitation of instruments, the wind characteristics are analyzed roughly. Mann *et al.* (1991) carried out the turbulence observation and spatial coherence study on Great Belt Bridge site in Danmark. Toriumi *et al.* (2000) conducted field measurements of typhoon wind at the Ohnaruto Bridge, and the Akashi-Kaikyo Bridge. But only the spatial correlation of natural wind is studied, the other wind characteristics such as the turbulence intensity and the turbulence integral length are not calculated. Xu and Zhu (2005) took the Tsing Ma suspension bridge during Typhoon Sam as an example to study the skew wind characteristics surrounding the bridge and the buffeting responses of the bridge under skew winds. The measurement auto-spectra of fluctuating wind speeds are compared with Kaimal spectrum, Simiu spectrum and von Karman spectrum and found out that the all those experience spectrum can not fit the test results well. Zhao *et al.* (2009) conducted the statistical analyse based on many years records of typhoon crossing Shanghai in China and found out that the serious variance of stochastic parameters in typhoon wind field can not be ignored and the assessment to typhoon disasters must be combined with reliability algorithm. Using Monte-Carlo method, the extreme wind speed and the wind profile were predicted. Wang *et al.* (2009) and Wang *et al.* (2010) summarized the characteristics of strong winds at the Runyang Suspension Bridge based on field tests from 2005 to 2008, but only a few strong winds including four typhoons and one northern wind are investigated. The difference between the measurement results and Kaimal spectrum is remarkable and the necessity of field test is highlighted. However, the wind database in China is far from insufficient because of the different geographical characteristics in different regions. Furthermore, almost all the researchers focused on extremely strong wind characteristics and its effect on structures. Sustained wind load is one of the key factors determining the life and fatigue stress amplitude of long-span bridges, and its impact on the buffeting response of long-span bridges can't be neglected also. Because of this, the study of sustained wind statistical characteristic is one of the fundamental subjects of wind-resistance engineering that should be reinforced.

The Runyang Suspension Bridge, as shown in Fig. 1, located on the south side is one of the two components of Runyang Yangtze River Bridge. It has the longest in China and the third longest in the world suspension span of 1490 m when it was opened in 2005. Because the first frequency of this bridge is only 0.04941Hz (Wang *et al.* 2009), the wind load effect is very significant. The study noted that the Runyang Suspension Bridge is located in the northern region of the subtropical zone, with obvious subtropical monsoon climate characteristics. The cold and dry

northern wind from the mainland is the main strong wind in winter, and in summer the typhoon dominates. The climate in the Runyang Suspension Bridge site is complex and there are many adverse weather events including typhoons, storms, and thunderstorms. All of these facts make a field study of wind characteristics on this long suspension bridge site of particular importance. As the basis of wind characteristics study, the field measurement for long-term wind field in the Runyang Suspension Bridge site is very necessary.

Based on the structural health monitoring system of the Runyang Suspension Bridge, more than five years field continuous wind data was obtained in the mid-span at the height of girder deck and south tower top respectively. One year field measurement results were selected for study in this paper. Taken 10 minutes as a basic interval, more than 10000 field measurement wind sub-samples were used for analyse. Using statistical method, the characteristics of mean wind and turbulence wind are presented in detail, and the relationships between wind characteristics are deduced. The turbulence spatial coherence analysis was conducted according to the measurement date from the two observation stations. The results from two locations are compared for validating the reliability of the measurement data and also compared with the recommended values in current long-span bridge design specification and results in other relevant studies. The research results not only are used for performance evaluation of the bridge, but also can be a supply for wind database of eastern China.

Fig. 1 Overview of Runyang Suspension Bridge

2. Wind environment monitoring subsystem of Runyang Suspension Bridge

The structural health monitoring system was installed on the Runyang Suspension Bridge to monitor the integrity, durability and reliability of the bridge. It has four sub-systems: sensory system, data acquisition and transferring system, data managing and controlling system, and structural health estimation system. The sensor subsystem includes anemometer, temperature sensor, displacement sensor, strain sensor, acceleration sensor, load sensor, and so on (Pakzad 2010, Ding and Li 2011). Two WA15 anemometers from the Vaisala Company (USA) were used in the SHMS. One of the WA15 anemometers was deployed in the middle of the main span (upstream) 69.300 m above the ground (station A) and the other on the top of the south tower (downstream) 218.905 m above ground (station B). The anemometers were installed to the north, originated the zero wind angle to wind blowing from the north. By the convention that positive rotation goes clockwise, east is 90°, and so on. The anemometer can be operated in the temperature range of -55-55℃. The range of the wind speed measurement was set from 0.4 m/s to

51.2 m/s, the resolution of the sensor is less than 0.1m/s, the sampling frequency was set 1 Hz, the data measured includes real time horizontal wind speed and wind direction. From now on, the anemometer has worked continuously more than 2200 hours. Five years successful application in meteorological study shows that the WA15 anemoscope can work under any kinds of bad weather and accurately acquire the wind speed and direction simultaneously. The cables carrying the analog output voltage proportional to wind speed and wind direction went through the inside mast to the data managing and controlling subsystem of the monitoring system.

For the airflow is disturbed by the bridge deck easily when the wind attacks the bridge, the anemometer should have enough distance from the bridge to obtain the real wind characteristics data. Therefore, the bracket is needed to fix the anemometer and make the anemometer apart from the bridge deck. If the bracket is not rigid enough, the anemometer will vibrate under strong wind. And too rigid bracket is uneconomic and not convenient to carry and install. So the bracket is designed carefully (Wang *et al.* 2009), as shown in Fig. 2. The anemometer is installed on the top of vertical rod and the vertical rod is fixed on the end of the horizontal rod. The vertical braces ensure the anemometer can not swing in vertical plane and the horizontal braces ensure the anemometer can not swing in horizontal plane. The stainless steel is chosen as the material of the bracket to maintain long-term reliability of the bracket. All components of the bracket are made up of round-pipe and can be disconnected and assembled easily. The length of horizontal rod is about 9 m.

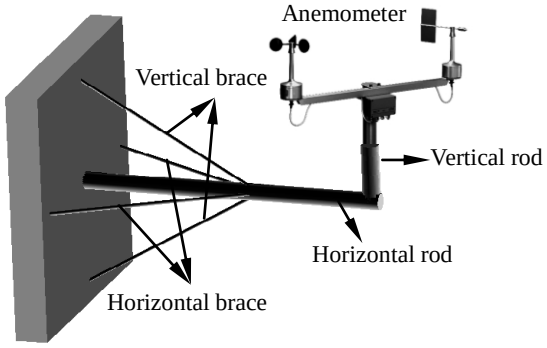

Fig. 2 The sketch of bracket

3. Statistical characteristics of field measurement sustained wind

The random natural wind can be decomposed into steady component and fluctuating component to convenient wind resistance research. The first part can be described by mean wind speed, direction, the wind speed variation with height, and the second part can be described by turbulence intensity, gust factor, turbulence integral scale, power spectral density, spatial correlation, etc.

In bridge wind engineering, the vector decomposition method is used for wind decomposition. The horizontal wind speed $U(t)$ and direction $\alpha(t)$ are directly measured from the anemometer.

Two perpendicular wind components in the north $U_N(t)$ and in the east $U_E(t)$ can be obtained using the following equation

$$U_N(t) = U(t)\cos\alpha(t) \tag{1}$$

$$U_E(t) = U(t)\sin\alpha(t) \tag{2}$$

The 10-min mean wind speed $\overline{U}$ can be calculated

$$\overline{U} = \sqrt{\overline{U}_N^2 + \overline{U}_E^2} \tag{3}$$

where $\overline{U}$ represents the 10 minutes mean wind speed, $\overline{U}_N$ and $\overline{U}_E$ represent the north and east 10 minutes mean wind speed respectively.

The corresponding mean wind direction $\overline{\alpha}$ is determined by the directional cosines of the mean wind speed

$$\overline{\alpha} = \arccos\left(\frac{\overline{U}_N}{\overline{U}}\right) \tag{4}$$

Finally, the components of fluctuating wind speed in longitudinal and lateral directions, $u(t)$ and $v(t)$, are respectively computed

$$u(t) = U_N\cos\overline{\alpha} + U_E\sin\overline{\alpha} - \overline{U} \tag{5}$$

$$v(t) = -U_N\sin\overline{\alpha} + U_E\cos\overline{\alpha} \tag{6}$$

3.1 Mean wind speed and direction

The mean wind characteristics include mean wind speed, wind direction corresponding with the mean wind speed and wind speed variation with height, which are the key factors determining the wind load value of structural design. The statistical mean wind speed characteristics of sustained wind can be used for forecasting the maximum 10 min wind speed of different return period in bridge site. Because of the long-span and flexibility of the Runyang Suspension Bridge, the influence of daily wind load on the performance of structure can not be neglected; the old Tacoma Bridge is a serious example.

The daily maximum 10-min mean wind speed of 275 days and its probability distribution are plotted in Figs. 3 and 4 for the data obtained from mid-span and tower top. The variation of wind speed with time can be clearly seen in Fig. 3. The mean wind speed in the mid-span is small than the tower top obviously. The daily maximum 10-min mean wind speed is not exceed 15 m/s except some special days even on the tower top, which is far less than the suggested value of bridge design specification and field measurement typhoon results (Toriumi *et al.* 2000, Xu *et al.* 2001,

Xu *et al.* 2007, Song *et al.* 2010). Numerical statistic results show that the average wind speeds of 275 days are 7.555 m/s and 10.196m/s at the height of main girder and tower top respectively. The maximum mean wind speeds are 20.327 m/s in the middle of the main span and 23.822 m/s on the top of south tower on August 5th 2005, the date that typhoon "Matsa" attacked the bridge. The two anemometers reach the maximum at the same time, as shown the circled points in Fig. 3, which validates the reliability of the measurement data. Influenced by the typhoon landing in summer and strong north wind in winter, the mean wind speed in the bridge site has high divergence; distributes from 2.00 m/s to 18.00 m/s in mid-span and 1.25 m/s to 21.25 m/s on tower top, as shown in Fig. 4. Therefore, the statistical analyze results based on long-term field measurement data can reveal the mean wind characteristics of Runyang Suspension Bridge site and contiguous region more accurate.

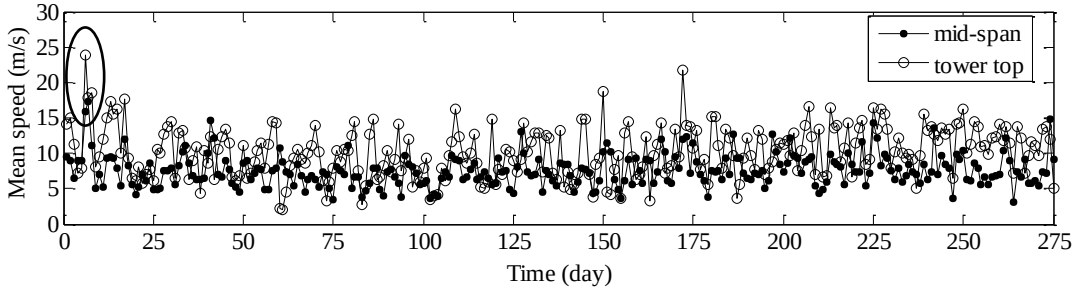

Fig. 3 Maximum daily 10 min mean wind speed of 265 days

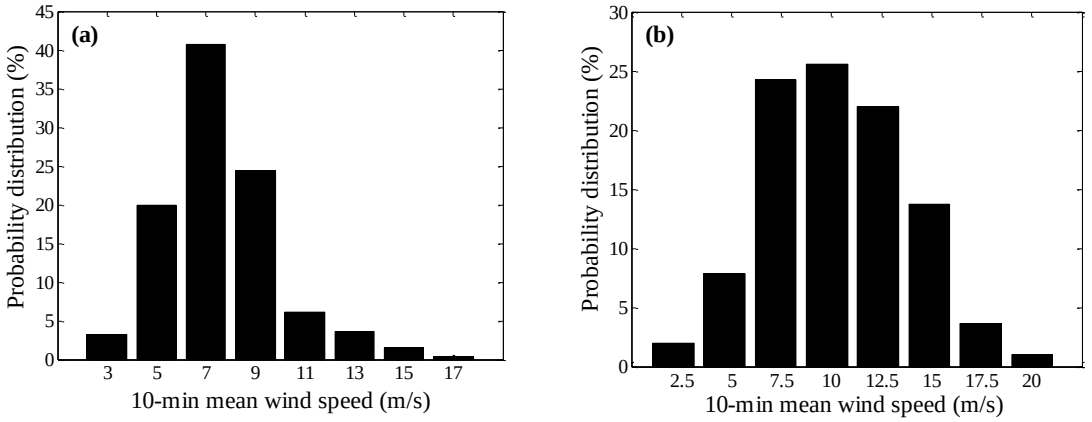

(a) mid-span (b) tower top

Fig. 4 Probability distribution of maximum day 10 min mean wind speed

Fig. 5 shows the wind rose in mid-span and tower top. As can be seen, the directions of daily maximum 10-min mean wind speed in mid-span are mainly east (E), southeast (SE) and south (S), and their distribution probabilities are 19.90%、20.98% and 18.90% respectively; the directions of

daily maximum 10 min mean wind speed on tower top are mainly east (E), southeast (SE) and south (S) too, and their distribution probabilities are 18.41%、18.74% and 17.76% respectively. The consistent distribution of direction in mid-span and on tower top also proves the validity of the two anemometers' measurement results. The bridge site is attacked by the airflow from southeast coast dominantly all one year, and swept by cold air from north in winter.

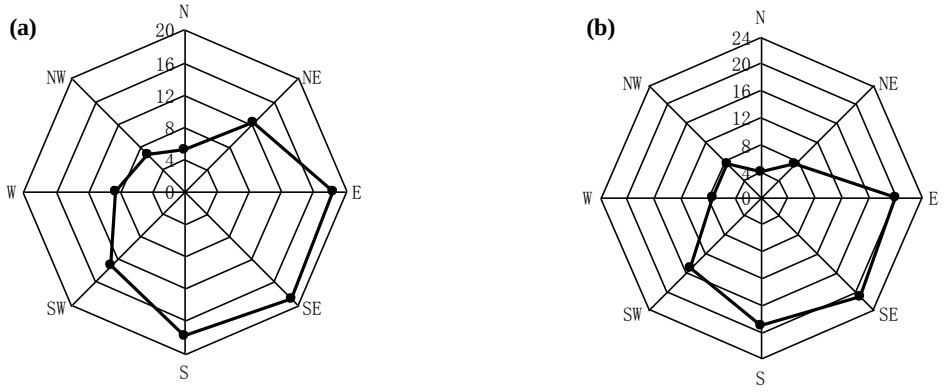

(a) mid-span (b) tower top

Fig. 5 Wind rose

The speed of airflow in the ground atmospheric boundary-layer is reduced by the hindrance of objects on the ground surface, and this effect of hindrance becomes weak with the height increasing. Therefore, the wind speed at different height is not uniform. In order to calculate wind load accurately in structural wind resistance design, the wind speed at different height must be determined. But field measuring wind speed at different height in different place is an impracticably task. As a consequence, researchers proposed the expression for the contour line of the wind speed based on theoretical deduction and experimental statistic studies. The exponential expression is a popular type used in many references and employed by Chinese bridge wind resistance design specification. The wind speed at different height is expressed as follows

$$\frac{U_2}{U_1}=\left(\frac{Z_2}{Z_1}\right)^{\alpha} \tag{7}$$

Where, U_1 and U_2 are wind speed at height Z_1 and Z_2, respectively; α is the dimensionless exponent influenced by the roughness of the ground.

Based on the 10-min mean wind speed at the height of main girder and tower top at corresponding time, more than 5000 samples of α are calculated using Eq. (7). The statistical result of index α is show in Fig. 6. The probability distribution is similar to normal distribution.

The value mainly concentrates on the range of 0.09-0.17; the distribution probability of value near 0.13 is more than 40%; the mean value is 0.1299, which is very close to the recommendatory

results of specification. Hence, the exponential expression can describe the wind speed variation with the height on the Runyang Suspension Bridge site even the height exceeding 200 m a little.

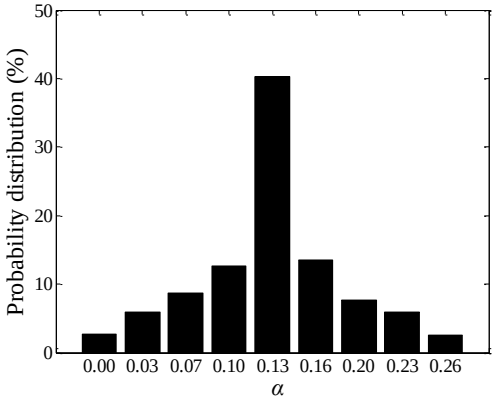

Fig. 6 Probability distribution of index α.

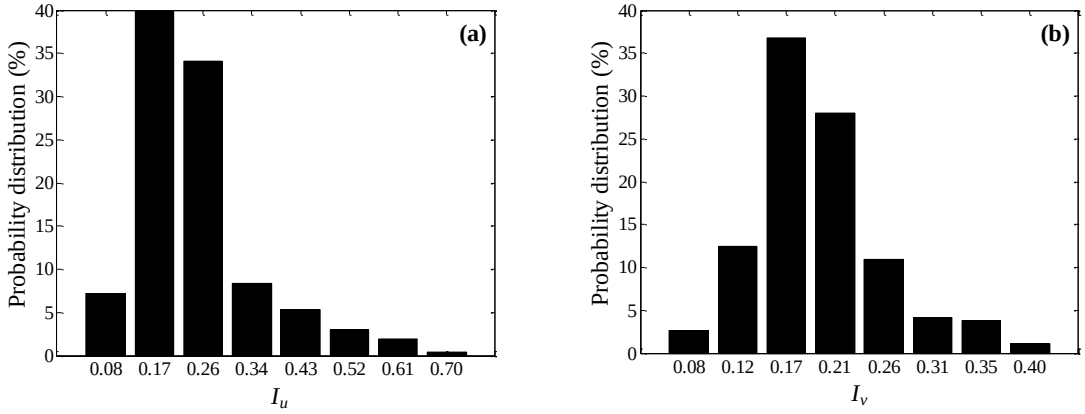

(a) longitudinal component (b) lateral component

Fig. 7 Probability distribution of measurement turbulence intensity (mid-span anemometer)

3.2 Turbulence intensity and gust factor

The turbulence intensity represents the intensity of wind fluctuation and is an important parameter that determines dynamic response of long-span bridges excited by fluctuating wind. The turbulence intensity is defined as the ratio of the standard deviation of fluctuating wind to mean wind speed for a given duration, seen in Eq. (8). The intensity of fluctuating wind can be described by gust factor too, but the two parameters represent the intensity of wind fluctuation from different aspects, therefore, the calculation method is different. The gust factors is defined as the ratio of the maximum gust speed in gust duration to mean wind speed, seen in Eq. (9). In structural wind engineering, 3 seconds are used as basic gust duration in general, and is also adopted in this paper.

$$I_u = \frac{\sigma_u}{U} \qquad I_v = \frac{\sigma_v}{U} \tag{8}$$

$$G_u(t_g) = 1 + \frac{\max[\overline{u(t_g)}]}{U} \qquad G_v(t_g) = \frac{\max[\overline{v(t_g)}]}{U} \tag{9}$$

where, I_u and I_v represent turbulence intensity of the fluctuating wind in two directions $u(t)$ and $v(t)$ respectively; σ_u and σ_v represent the root-mean-square values of $u(t)$ and $v(t)$ respectively; $G_u(t_g)$ and $G_v(t_g)$ represent turbulence intensity of the fluctuating wind in two directions $u(t)$ and $v(t)$ respectively; $\overline{u(t_g)}$ and $\overline{v(t_g)}$ represent the average wind speed in gust duration (t_g) of $u(t)$ and $v(t)$ components respectively; U represents the 10 min mean wind speed.

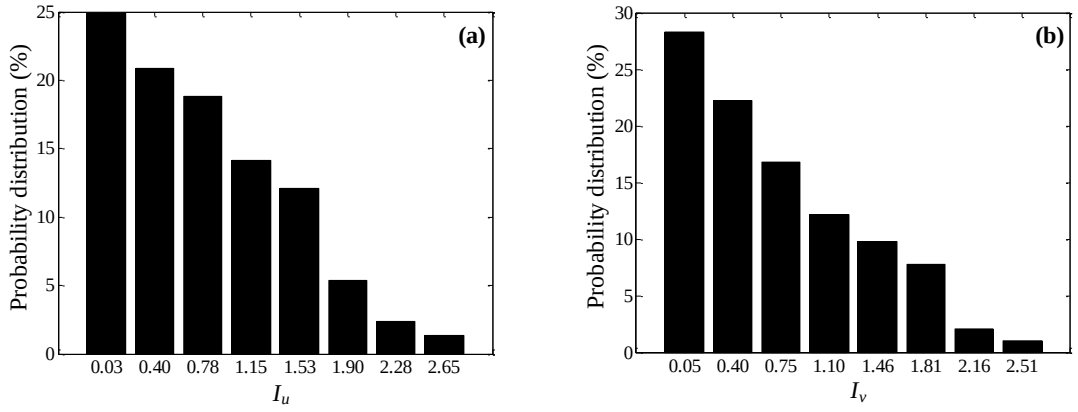

(a) longitudinal component (b) lateral component

Fig. 8 Probability distribution of measurement turbulence intensity (tower top anemometer)

Figs. 7 and 8 show the probability density distributions of measured turbulence intensity in mid-span and tower top respectively. It can be seen that the distribution regularity of turbulence intensity in mid-span is obviously different with that on tower top. In mid-span, the value of high distribution probability is in the middle of data range. But on tower top, the smaller of the turbulence intensity, the higher the distribution probability. It proves that the turbulence intensity has large randomness even in one bridge. This difference may be caused by that main girder has smaller impacts on the air flowing than the bridge tower, because the shape of transverse section of main girder is optimized based on the aerodynamics theory but that of tower is not optimized. The probability density distribution of measured gust factor has the similar regulation, as shown in Figs. 9 and 10, although the calculated equation is different. The turbulent wind characteristics distribution of longitudinal component and lateral component at the same height are coincident.

Therefore, for large scale structure, only the statistical results deduced from long-term field measurement data in different places of one structure can describe the wind characteristics on this structure site actually. Furthermore, the measurement results have a close relationship with the environment where the anemometer is located on. The importance of structural health monitoring system is highlighted.

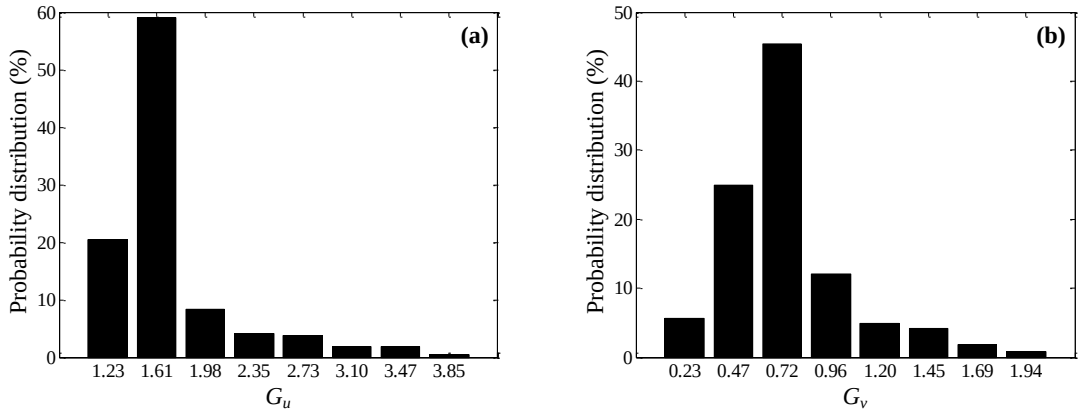

(a) longitudinal component (b) lateral component

Fig. 9 Probability distribution of measurement gust factor (mid-span anemometer)

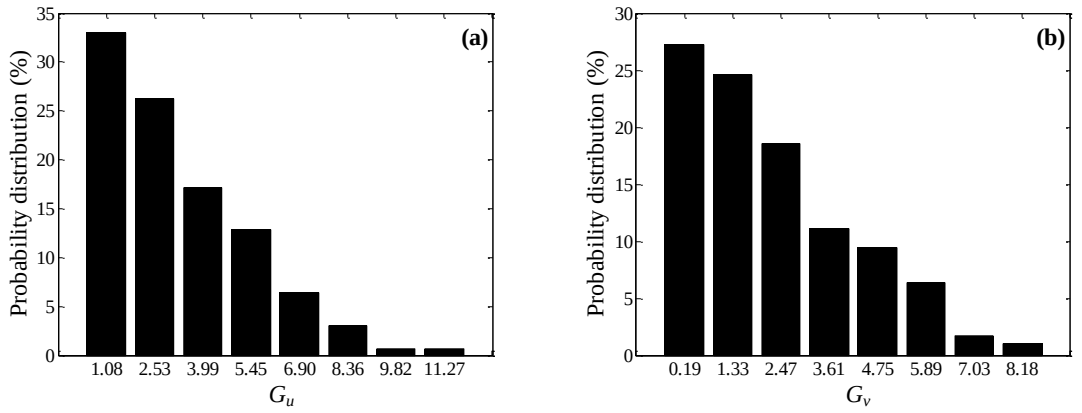

(a) longitudinal component (b) lateral component

Fig. 10 Probability distribution of measurement gust factor (tower top anemometer)

Numerical analysis results indicate that, in mid-span, the average longitudinal and lateral turbulence intensities are 0.240 and 0.203 respectively, and the average longitudinal and lateral gust factors are 1.737 and 0.799 respectively; on tower top, the average longitudinal and lateral turbulence intensities are 0.817 and 0.745 respectively, and the average longitudinal and lateral gust factors are 3.402 and 2.429 respectively. The turbulence intensity is much larger than the Typhoon and strong north wind (Wang *et al.* 2010). Average values of the turbulence intensity in

mid-span is much smaller than these on tower top, which is not obey the general regulation that it has the big value of turbulence intensity near ground surface. In the specification, the recommended values of turbulence intensity are 0.11 at the height of main girder and 0.10 at the height of tower top. The measurement results are much larger than recommended values especially on tower top, so the suitability of the specification about the turbulence intensity needs further confirmation.

Based on large amount of data, the correlations between the turbulence parameters and 10-min mean wind speed can be revealed. Fig. 11 gives the relationships between the lateral turbulence intensity and longitudinal turbulence intensity in the two stations. The linearity of the two directional components is very good. The lateral turbulence intensity increases with the longitudinal turbulence intensity increasing, which shows that fluctuating wind is three-dimensional, and the disturbance from one direction to the wind will influence the air flowing of other two directions. Based on linear fitting method, the scale relationship can be expressed as I_v=0.599I_u-0.058 (in mid-span) and I_v=0.921I_u-0.006 (on tower top). Neglecting the residue because of its small value, the equation can be simplified as I_v=0.599I_u (in mid-span) and I_v=0.921I_u (on tower top). Comparing with reference (Wang *et al*. 2010), only the result of tower top is coincident with the results of typhoon "Matsa" (I_v=0.95I_u), "Khanun" (I_v=0.98I_u) and "Wipha" (I_v=0.95I_u), the proportionality coefficient in the middle span is much small. It is because that the sustained air flowing orientation is very close the longitudinal direction of main beam and the wind speed in middle span is small, which induces inconspicuous lateral fluctuation wind. Therefore, the environmental factors including surface roughness, structures on the ground, the geographical position of bridge site and terrain feature influence the turbulent characteristics of sustained wind. The specification suggested expression is I_v=0.88I_u when there is no data measurements, the coefficient is between that of mid-span and tower top. From the analyzing, it is obvious that the current specification is not completely suited for the RSB in respect of turbulence intensity.

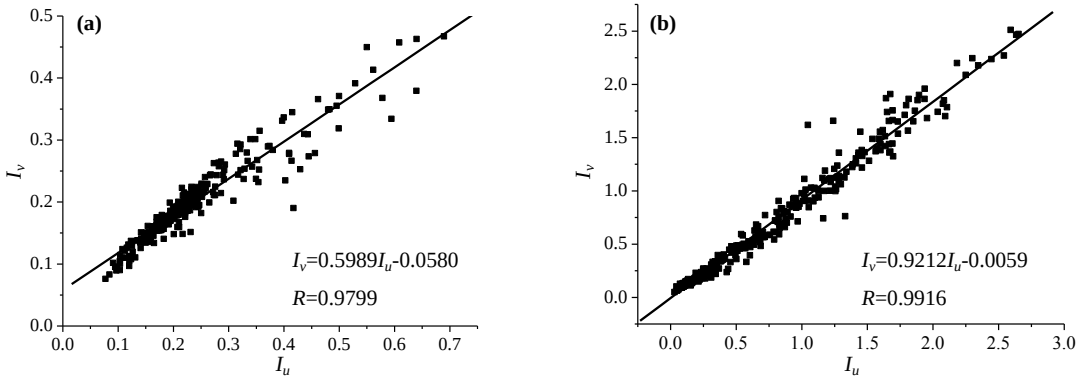

(a) mid-span (b) tower top

Fig. 11 The lateral turbulence intensity vs. the longitudinal turbulence intensity

The gust factors between the lateral component and longitudinal component have relevance too, as can be seen in Fig. 12. In middle span, the small value area and big value area show different linearity. The linearity on tower top is better.

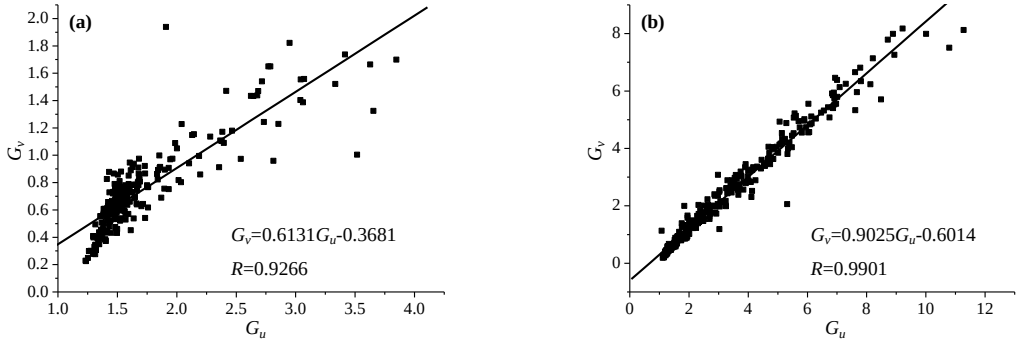

(a) mid-span (b) tower top

Fig. 12 The lateral gust factor vs. the longitudinal gust factor

Not only that, although the turbulence intensity and gust factor calculated using different equations, the turbulence intensity has correlation with the gust factor, which shows in Fig. 12 and Fig. 14. At the same height, the proportional coefficient of turbulence intensity and gust factor is approximately equal.

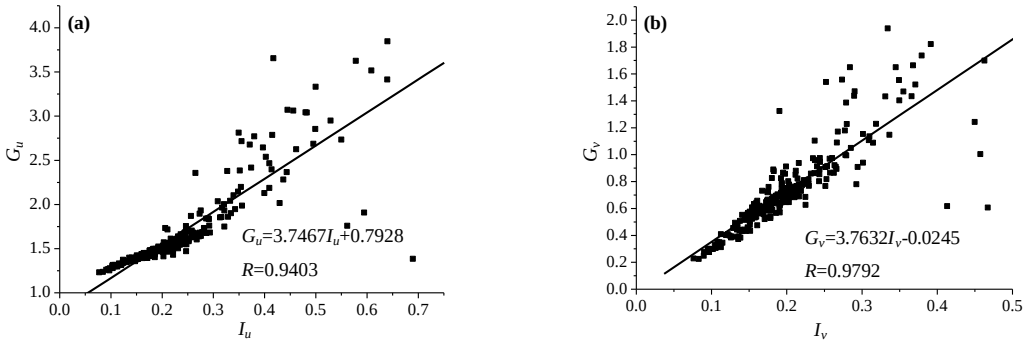

(a) longitudinal component; (b) lateral component

Fig. 13 The gust factor vs. the turbulence intensity (mid-span anemometer)

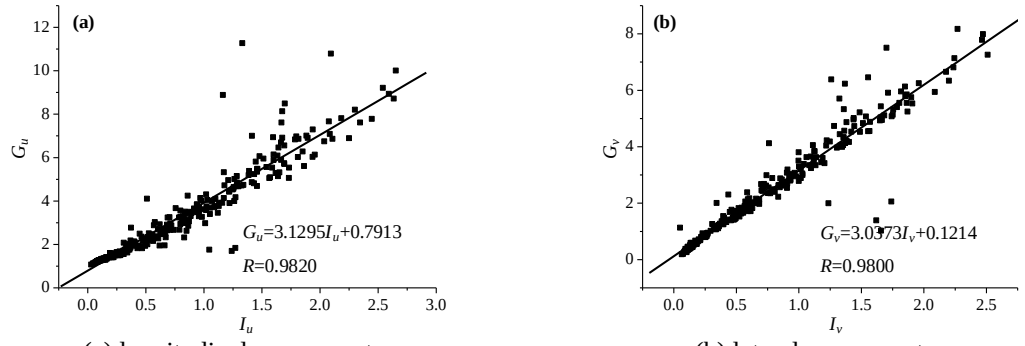

(a) longitudinal component (b) lateral component

Fig. 14 The gust factor vs. the turbulence intensity (tower top anemometer).

As usual, the fluctuating wind beneath the border layer of the atmosphere is mainly induced by the interference of objects on the ground, and does not have inevitable relation with the mean wind. However, from the relationship of turbulence intensity and mean wind speed shown in Fig. 15 and Fig. 16, it can be concluded that the turbulence intensity has the decrease tendency with the mean wind speed increasing when the height over the ground is high enough that the roughness influence does not dominate. Therefore, with the mean wind speed increasing, the air flowing becomes more steady and can not be disturbed by obstruction on the ground.

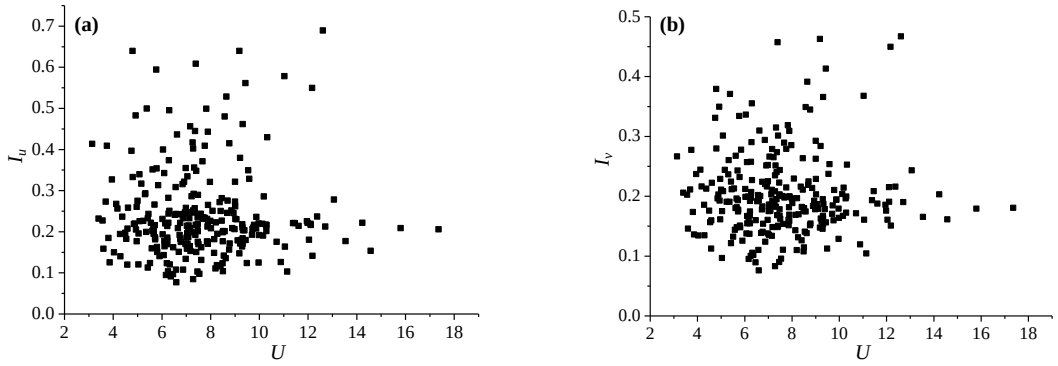

(a) longitudinal component (b) lateral component

Fig.15 The turbulence intensity vs. 10-min mean wind speed (mid-span anemometer)

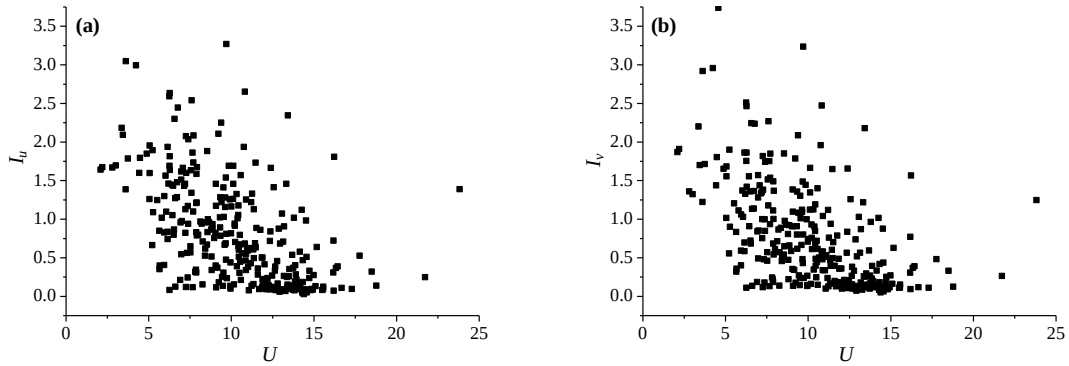

(a) longitudinal component (b) lateral component

Fig.16 The turbulence intensity vs. 10-min mean wind speed (tower top anemometer)

3.3 Turbulence integral length

The fluctuating wind can be considered to be caused by a superposition of conception eddies. The turbulence integral length is a measure of the average size of the turbulence eddies in the direction of the mean flow. The turbulence integral length is a very important parameter in

structural wind engineering. For example, if the scale of the turbulence eddy is bigger than the scale of the structure, the fluctuating response of the structure induced by turbulence wind in different place will superpose, otherwise the response will counteract. According to the Taylor's hypothesis, the longitudinal turbulence integral length can be calculated as follow

$$L_u^x = \frac{U}{\sigma_u^2}\int_0^\infty R_u(\tau)d\tau \tag{10}$$

where, L_u^x is turbulence integral length, U is 10 min mean wind speed, σ_u the standard deviation of fluctuating wind, $R_u(\tau)$ is the autocorrelation of fluctuation wind. Based on the conclusion deduced by Flay and Stevenson (1998), the best upper limit of the integral is the value of τ when the corresponding $R_u(\tau)$ monotonically descends to $0.05\sigma_u^2$.

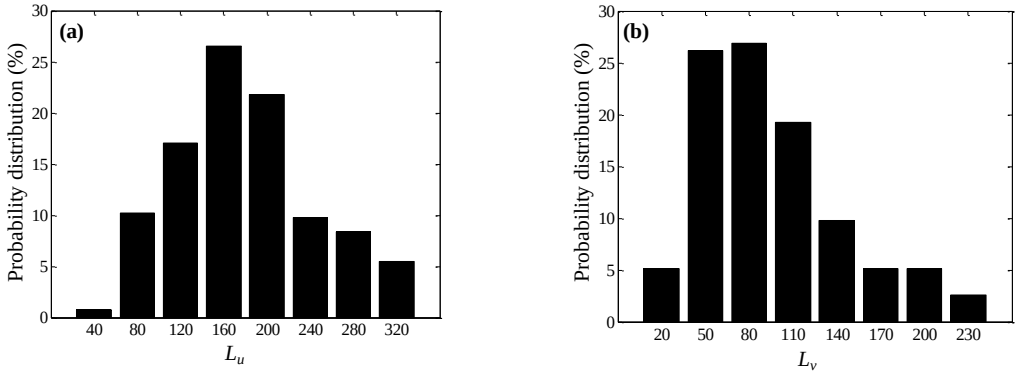

(a) longitudinal component (a) longitudinal component

Fig. 17 Probability distribution of measurement turbulence integral length (mid-span anemometer)

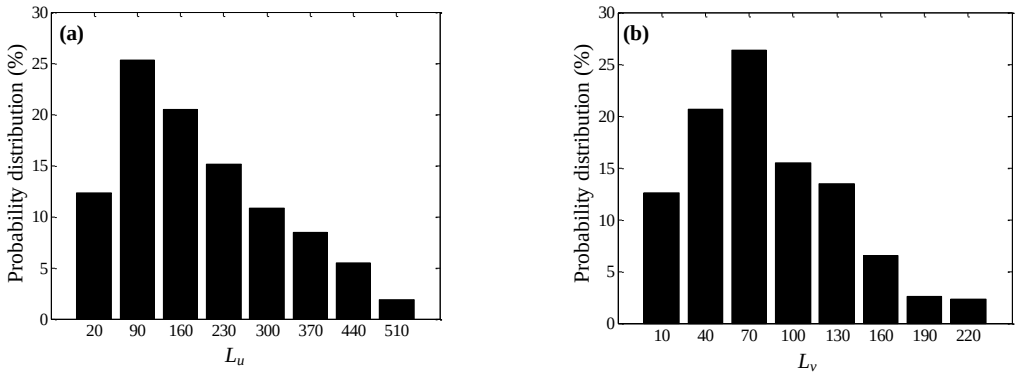

(a) longitudinal component (b) lateral component

Fig. 18 Probability distribution of measurement turbulence integral length (tower top anemometer)

Figs. 17 and 18 show the probability distributions of turbulence integral length. All of the four results can be described by Gaussian distribution although the value of turbulence integral length is various. Numerical statistical results of the turbulence integral length are listed in Table 1. The average longitudinal turbulence integral length in mid-span is smaller than that on tower top, but the average lateral turbulence integral length in mid-span is larger than that on tower top. From Table 1, it is very clear that the average turbulence integral lengths at different altitude change intensively and all the values are larger than suggestion values in specification except for the lateral turbulence integral length on tower top. Comparing with the specification, the air flowing is more steady at main girder height and more fluctuation at tower top height. It means that there is a possibility to ease the design specification of long span bridge concerning the turbulence integral length at the height of main girder; but at height of tower top, it should be tightened.

Table 1 Statistical results of turbulence integral length (Unit: m)

Item	Mid-span		Tower top	
	L_u	L_v	L_u	L_v
Maximum value	432.33	352.33	690.10	247.37
Minimum value	25.34	21.56	2.73	1.09
Average value	178.05	95.95	227.02	72.70
Standard deviation	68.70	51.74	174.98	58.97
Specification value	120	60	180	90
Ratio (Average value/ Specification value)	1.48	1.60	1.26	0.81

Similar with other turbulence parameters, the turbulence integral length of longitudinal component and lateral component has strong relationship as shown in Fig. 19. According to linearity fitting, the relationship can be expressed as $L_v = 0.6078L_u - 12.7853$ in mid-span and $L_v = 0.3109L_u + 4.3208$ on tower top.

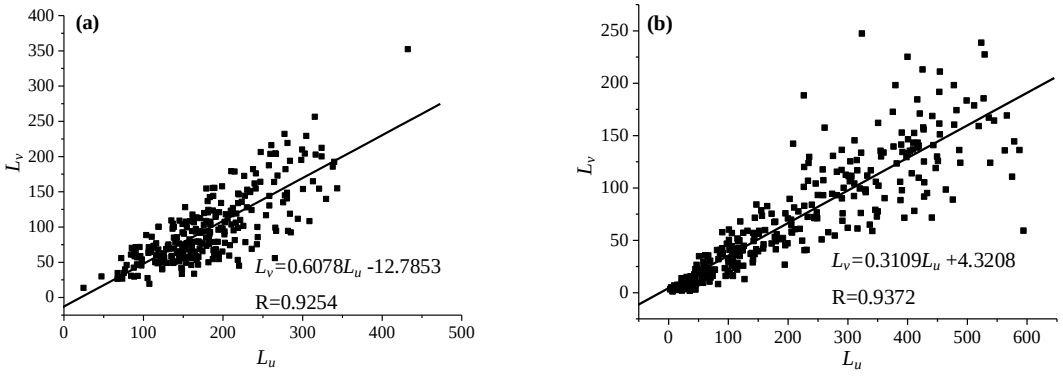

(a) mid-span (b) tower top.

Fig. 19 The lateral turbulence integral length vs. the longitudinal turbulence integral length

Figs. 20 and 21 plot the correlations of turbulence integral length and turbulence intensity. As can be seen, although the two parameters have different physical meaning, the relationship can still be deduced from a large number of samples no matter longitudinal component or lateral component. This type of regulation obtained from tower top test data is more clear. The turbulence integral length decreases with the turbulence intensity increasing. The turbulence integral length also has some relationship with the mean wind speed. Figs. 22 and 23 show the relationships between turbulence integral length and mean wind speed. It is found that there is a tendency for the turbulence integral length to ascend with mean wind speed increasing. In the condition of low wind speed, the big turbulence eddies breaks into small size turbulence eddies rapidly, which induced strong fluctuating characteristics of air flow.

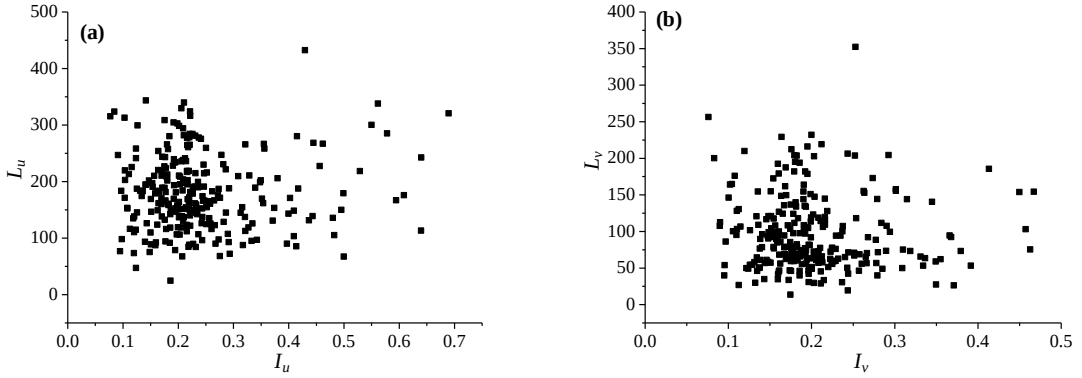

(a) longitudinal component (b) lateral component

Fig. 20 The turbulence integral length vs. the turbulence intensity (mid-span anemometer)

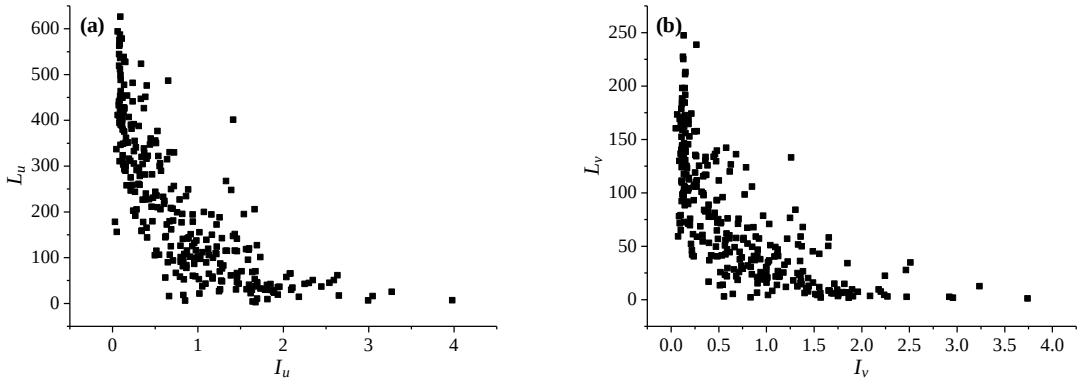

(a) longitudinal component (b) lateral component

Fig. 21 The turbulence integral length vs. the turbulence intensity (tower top anemometer)

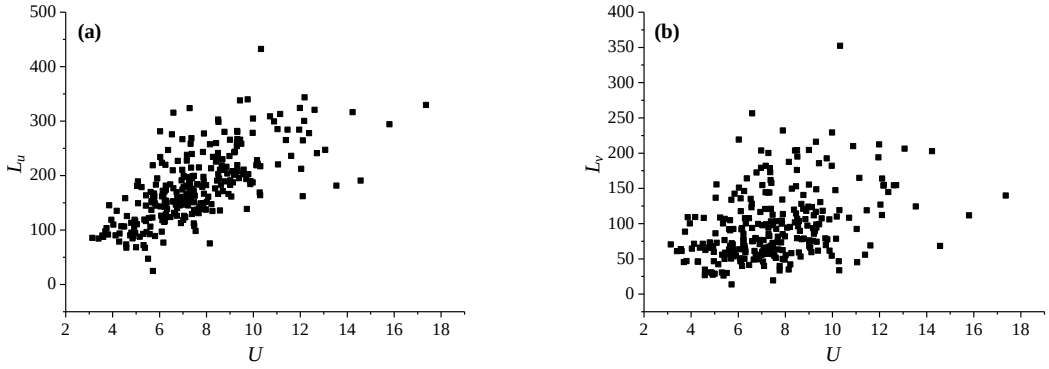

(a) longitudinal component (b) lateral component

Fig. 22 The turbulence integral length vs. the 10-min mean wind speed (mid-span anemometer).

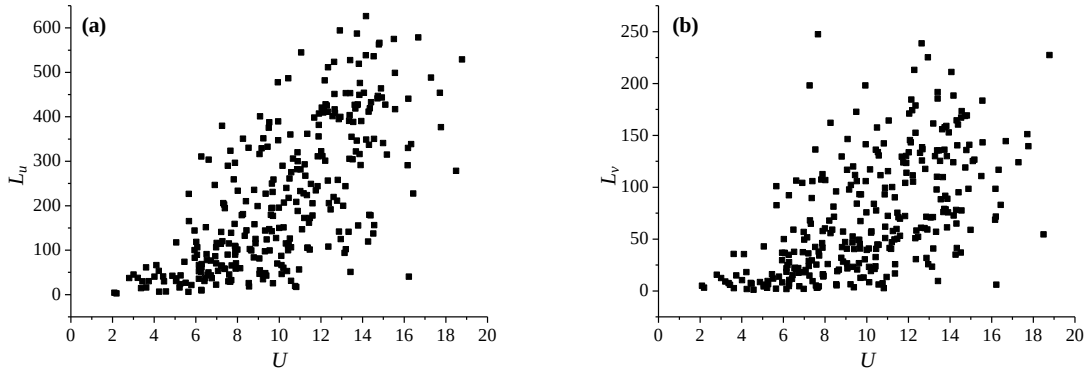

(a) longitudinal component (b) lateral component

Fig. 23 The turbulence integral length vs. the 10-min mean wind speed (tower top anemometer)

When overall comparing the characteristics of turbulence parameters in mid-span with that on tower top in Figs. 12, 15, 16 , 20, 21, 22 and 23, it can be concluded that the fluctuating wind field in the mid-span is controlled by the roughness of the ground, and the characteristics of fluctuating parameters are in random manner; the fluctuating wind field in the position of tower top has good regulation because of the seldom obstacles at this height. Therefore, for aerodynamic study, it is better to choose high open area as field investigation station.

3.4 Auto power spectral density

As one of the key turbulence characteristics, the auto power spectral density describes wind energy distribution over frequency and is the basis of wind field simulation. One important method for acquiring the turbulence power spectral density is to carry out the least-square fitting function based on extensive wind measurement records. There are many engineering functions for turbulence power spectral density model. The Chinese design specification for bridge engineering

displine has chosen the friction velocity normalized Simiu spectrum in horizontal direction. The along-wind turbulence wind power spectrum of mean wind speed U in the height Z can be expressed as

$$\frac{nS_i(n)}{(u^*)^2} = \frac{200f}{(1+50f)^{5/3}} \qquad i = u, v \tag{11}$$

where, $S_i(n)$ represents the power spectral densities; $i = u, v$ represents the longitudinal components and lateral components of fluctuating wind; n represents the frequency; $f = nZ/U$ means Monin coordinate; u^* represents the wind friction speed; Because there are no data measurements of u^* in the field wind test of the RSB, the value of u* can be calculated by the energy unitary method as

$$\sigma_i^2 = 6(u^*)^2 \qquad i = u, v \tag{12}$$

The von-Karman velocity spectrum is one that is usually used to fit the measured spectra for estimation of the integral scale using turbulence integral length as the fitting parameter. This method has the advantage of fitting the whole spectrum rather than only the position of the peak, so the von Karman spectrum is also employed for comparision. The von Karman spectrum has the form of (Morfiadakis *et al*. 1995)

$$\frac{nS_u(n)}{(\sigma_u)^2} = \frac{4L_u n/U}{[1+70.8(L_u n/U)^2]^{5/6}} \tag{13}$$

$$\frac{nS_v(n)}{(\sigma_v)^2} = \frac{4L_v n[1+755.2(L_v n/U)^2]}{U[1+283.2(L_v n/U)^2]^{11/6}} \tag{14}$$

where, $S_u(n)$ and $S_v(n)$ represent the longitudinal and lateral power spectral densities respectively, L_u and L_v represent the longitudinal and lateral turbulence integral length respectively, the meaning of other symbols is the same as Eq. (11).

The Simiu spectrum and Von Karman-type spectrum have been used to fit the measured spectra for the purpose of estimating the energy distribution of the wind measured on Runyang Suspension Bridge site both in mid-span and on tower top. The frequency resolution used for analyse is 0.000278 Hz. Figs. 24 and 25 show the normalized spectrum of fluctuating wind on the basis of the measured data sustaining one year in the two stations respectively. The spectrum estimated using Simiu spectrum and Von Karman-type spectrum are also presented in Figs. 24 and 25 for comparison purposes. It can be seen that the shape of power spectrum of fluctuating wind in the bridge site does not agree with the Simiu spectrum and Von Karman spectrum in all the four conditions. The longitudinal spectrum and lateral spectrum of measurement wind are not coincident too. Comparing with the measurement spectrum and Simiu spectrum, the measurement energy is smaller in low frequency range and is larger in high frequency range. The shape of von Karman spectrum is more close to the measurement results for the longitudinal component. From Figs. 24(b) and 25(b), it can be seen that much energy distributes in the high frequency range,

which is different with general wind power spectrum. Therefore, the accurate power spectrum model suitable for the bridge site needs further research. The parameters in power spectrum are studied by statistical method in next paragraph.

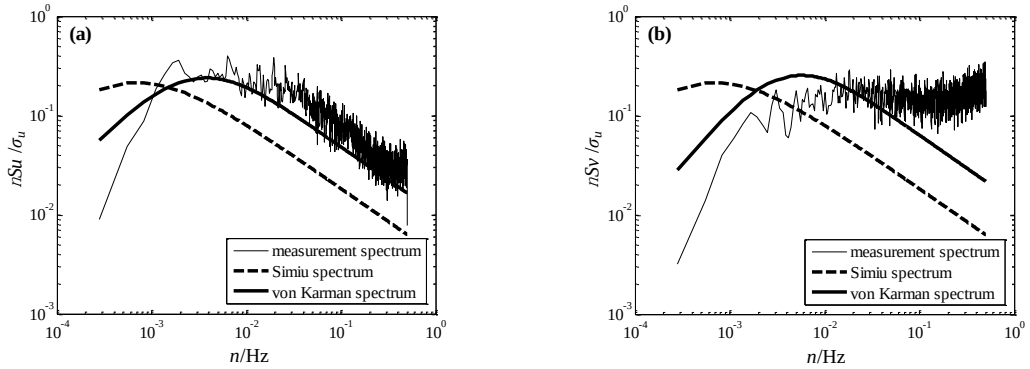

(a) longitudinal component (b) lateral component

Fig. 24 Wind auto-spectra (mid-span anemometer)

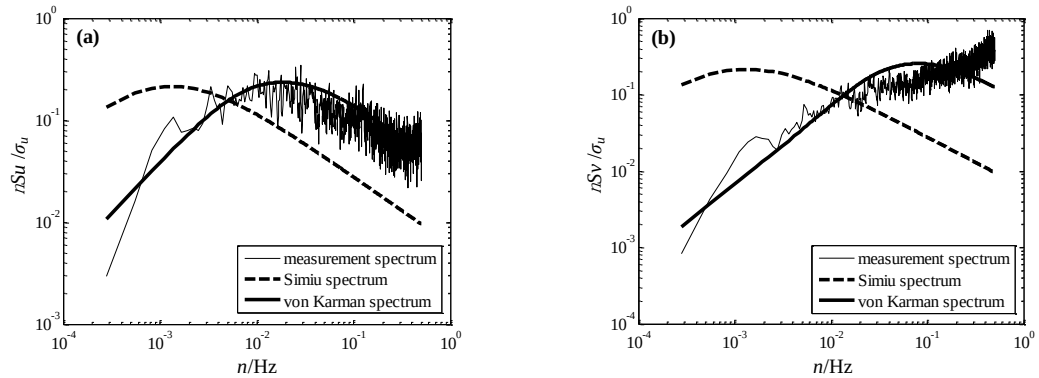

(a) longitudinal component (b) lateral component

Fig. 25 Wind auto-spectra (tower top anemometer)

Considering the importance of the fluctuating wind power spectrum in structural wind resistance design and wind field simulation, it is very necessary to study the parameters in power spectrum model. We suggest that the power spectrum equation both longitudinal component and lateral component should be expressed as

$$\frac{nS_i(n)}{\sigma_i^{\,2}} = \frac{Af}{6(1+Bf)^{\theta}} \tag{15}$$

where, the parameters A、B and θ can be obtain by least square fitting method based on the measurement data.

Figs. 26-29 show the fitting results of parameters A and B change with the mean wind speed both in mid-span and tower top. As can be seen, the parameters A and B have the ascending tendency with the mean wind speed increasing. This type of tendency is more obvious in the results calculated from tower top measurement data. The results obtained from mid-span data is jumbled because of the disturbing of obstacles on the ground. The statistical characters of index θ are shown in Figs. 30 and 31.The four figures have homologous feature. The probability distribution of the index is discrete, the value changes from 0.67 to 2.66. Therefore, utilizing a certain value of parameters A、B and θ to descirbe the power spectrum characteristics is not appropriate. The computing formulas of parameters A and B must consider the mean wind speed.

How to determine the relationship of parameters A、B and θ with mean wind speed needs further research.

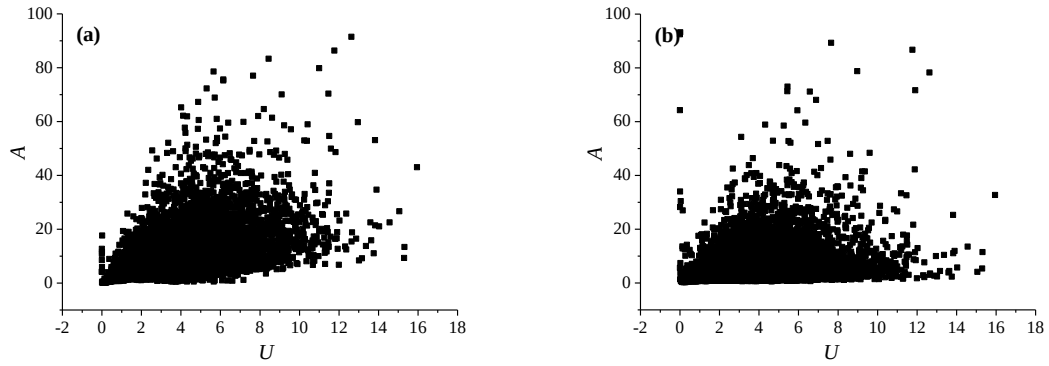

(a) longitudinal component (b) lateral component

Fig. 26 The parameter A of auto-spectra vs. the 10-min mean wind speed (mid-span anemometer)

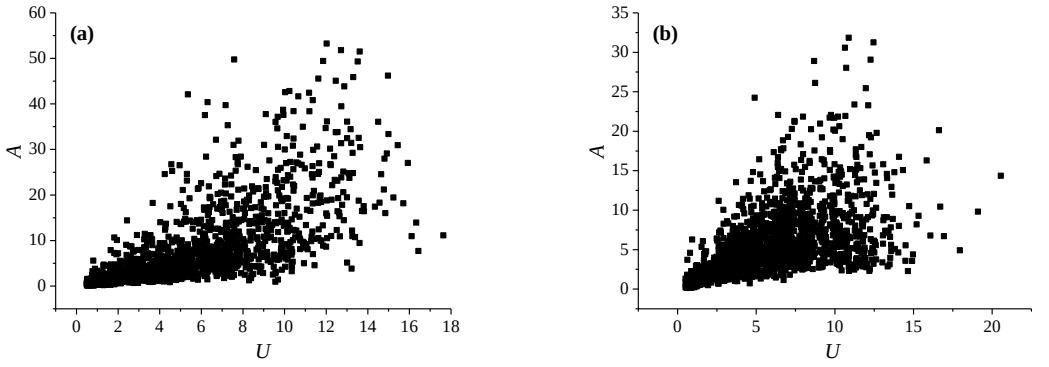

(a) longitudinal component (b) lateral component

Fig. 27 The parameter A of auto-spectra vs. the 10-min mean wind speed (tower top anemometer)

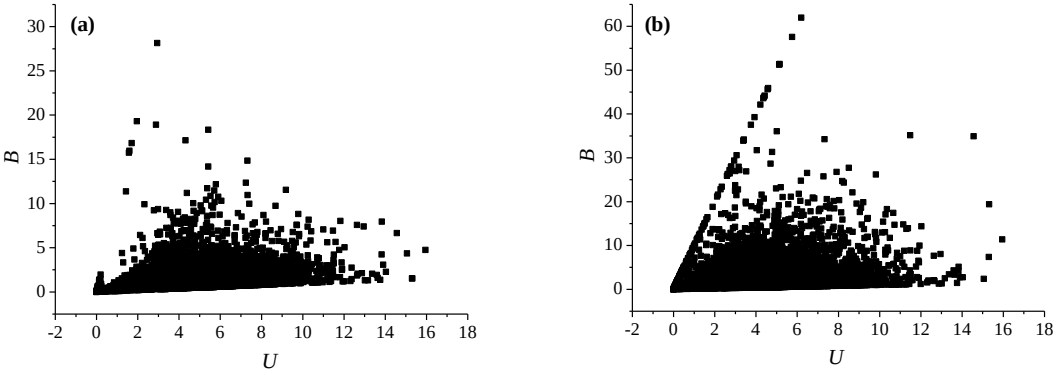

(a) longitudinal component (b) lateral component

Fig. 28 The parameter B of auto-spectra vs. the 10-min mean wind speed (mid-span anemometer)

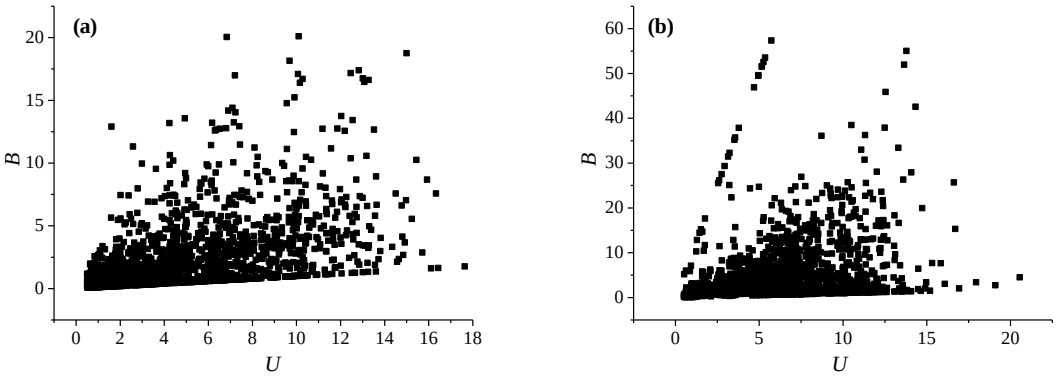

(a) longitudinal component (b) lateral component

Fig. 29 The parameter *B* of auto-spectra vs. the 10-min mean wind speed (tower top anemometer)

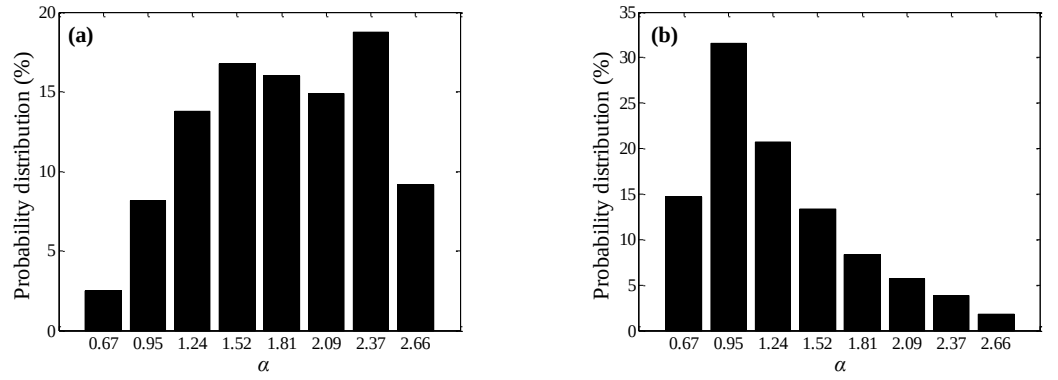

(a) longitudinal component (b) lateral component

Fig. 30 Probability distribution of auto-spectra parameter α (mid-span anemometer)

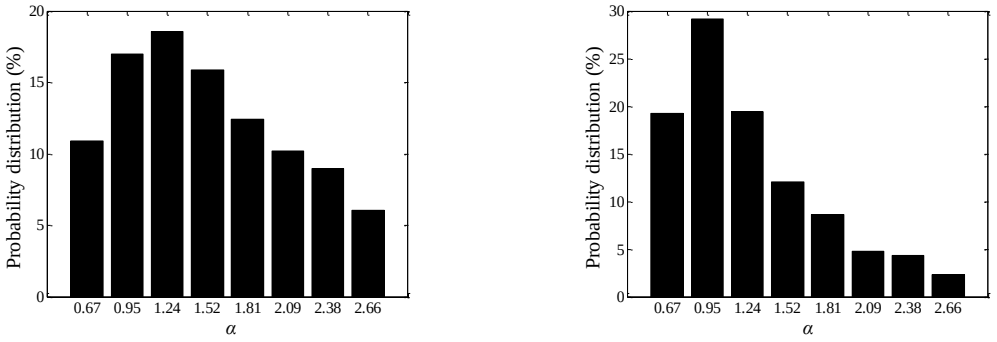

(a) longitudinal component (b) lateral component

Fig. 31 Probability distribution of auto-spectra parameter α (tower top anemometer)

3.5 Spatial correlation

The fluctuating wind characteristics are described not only by autocorrelation but also by spatial correlation. Strong wind records indicated that the wind speed and wind direction in different positions are not synchronous, and even independent completely. The wind induced response in different parts of the same long-span bridge seldom reaches to the maximum value simultaneously. If every part of the structure is designed according to the maximum wind load, the materials will be wasted. Therefore, the spatial correlation of field wind measurement is very important for wind field simulation. For structure with large horizontal scale and large vertical scale, the spatial correlation of two positions $A(z_1, x_1)$ and $B(z_2, x_2)$ is represented by co-coherence spectrum function. Longitudinal co-coherence spectrum function of fluctuation wind is often expressed by an exponential function, based on a report by Davenport (Simiu and Scanlan, 1996)

$$\rho(n, z_1, z_2, x_1, x_2) = \frac{S_{uu}^{C}(n, z_1, z_2, x_1, x_2)}{\sqrt{S_{uu}(n, z_1, x_1) S_{uu}(n, z_2, x_2)}} = \exp\left\{\frac{-n[C_z^2(z_1 - z_2)^2 + C_x^2(x_1 - x_2)^2]^{\frac{1}{2}}}{\overline{v_z}}\right\} \quad (16)$$

where, n is frequency, $S_{uu}^{C}(n, z_1, z_2, x_1, x_2)$ is the real part of the longitudinal cross-power spectrum, $S_{uu}(n, z_1, x_1)$ and $S_{uu}(n, z_2, x_2)$ are the longitudinal auto-power spectrum of position *A* and *B* respectively, C_z and C_x are the decay factors in *z* direction and *x* direction respectively and equal to 10 and 16 respectively suggested by Emil (Simiu and Scanlan 1996), $\overline{v_z}$ is the average wind velocity of 10 min mean wind speed at the height of z_1 and 10 min mean wind speed at the height of z_2. The measurement co-coherence in the Runyang Suspension Bridge site and the results of theoretical method proposed by Davenport are plotted in Fig. 32. The co-coherence of field measurement descends with the frequency increasing. Because of the low wind speed and long distance, the low frequency portion is disturbed easily than the high frequency portion. Therefore, the wind fields at two position of horizontal distance 745 m are almost independent. The measurement co-coherence in low frequency portion is much smaller

than the theoretical results. Combining with the test results at the Ohnaruto Bridge and the Akashi-Kaikyo Bridge (Toriumia *et al.* 2000), it can be suggested that the spatial correlation of natural wind in the theoretical results is overestimated in low frequency portion in some case. Anyway, the measurement co-coherence is very small and can be neglected, which indicated that the spatial correlation is very weak at the horizontal distance of 745 m.

Table 2 The comparison of wind characteristics

Parameters	Mean wind speed (m/s)	Turbulence intensity (%)		Gust factor		Turbulence integral length (Unite: m)	
		longitudinal component	lateral component	longitudinal component	lateral component	longitudinal component	lateral component
Sustain wind at the RSB mid-span	7.56	24.01	20.33	1.74	0.80	178.05	95.95
Sustain wind at the RSB tower top	10.20	81.74	74.52	3.40	2.43	227.02	72.70
Typhoon Matsa at the RSB mid-span	17.86 (max)	10.95	10.44	—	—	68.4	35.6
Typhoon Khanun at the RSB mid-span	11.13 (max)	21.31	20.98	—	—	116.4	52.2
Typhoon Wipha at the RSB mid-span	13.43 (max)	19.72	18.66	—	—	119.7	77.6
Typhoon Fung-Wong at the RSB mid-span	15.36 (max)	11.34	11.42	—	—	132.2	58.1
Northern wind at the RSB mid-span	10.91 (max)	16.02	14.22	—	—	99.6	48.1
Typhoon York at Di Wang tower	35.6 (max)	14.6	—	—	—	—	—
Typhoon Hagupit in Guangdong Province of China (before landfalling)	15.58	63	57	3.01	1.47	—	—
Typhoon Hagupit in Guangdong Province of China (after landfalling)	17.74	20	11	1.28	0.84	—	—
Typhoon Jelawat in Shanghai of China	7.73	28.9	22.9	1.73	0.63	78	—
Typhoon Prapiroon in Shanghai of China	9.53	33.3	30.3	1.90	0.86	78	—
Typhoon Chanzhu	22.01 (max)	16	10	1.36	—	97.8	62.1
Typhoon Sally	22.34 (max)	12	11	1.27	—	315.6	189.0
Typhoon Krosa at Shanghai World Financial Center of China	23.3	14.0	7.2	1.22	0.12	288.8	182.2

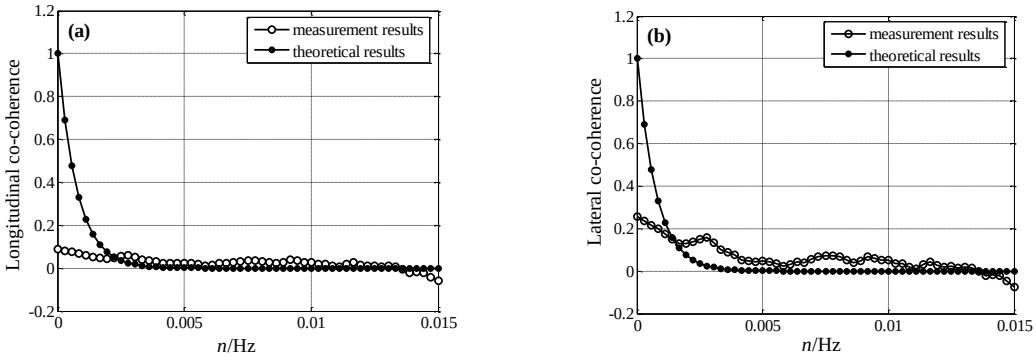

(a) longitudinal component (b) lateral component

Fig. 32 Co-coherence spectrum function

3.6 Comparison

Comparing the characteristics of sustained wind at the RSB with strong wind at the RSB and other places (Xu, *et al* (2001), Xiao *et al.* (2009), Wang *et al.* (2010), Li *et al.* (2010), Wu *et al.* (2010)), the results are listed in Table.2. It can be seen that the turbulence intensity and the gust factor are much stronger than most of strong wind especially on tower top although its mean wind speed is lower. Even in the same place, the turbulence characteristics are more obvious than strong wind. The turbulence integral lengths are bigger than all of the Typhoon except the Typhoon Krosa and the Typhoon Sally. That's because the heights of measurement location of the Typhoon Krosa and the Typhoon Sally are 436m and 335 m respectively and the measurement location heights of other typhoons are much smaller. It can be deduced that the height of measurement location has much influence on the values of wind characteristics.

4 Conclusions

The extremely strong wind induced responses are very important to low stiffness structures, the damage induced by sustained fluctuating wind can not be ignored too. The long-term field measurement wind data can be used for study the wind characteristics of the structural site and provide references for structural wind resistance design in contiguous regions. Structural health monitoring system can supply long-term reliable measurement wind data, which is the basis of research on the wind characteristics at bridge site. Based on one year field measurement records, the statistical analysis results of wind environment indicate that:

(1) The long-term mean wind speed is small both in mid-span and tower top. The 10-min mean wind speed on tower top is higher than that in mid-span. The wind in the mid-span mainly comes from east, southeast and south that is generated by the landing of southeast coastal airflow, which is coincidence with the results on tower top. The regulation of mean wind speed variation with height obeys the rule of Chinese bridge design specification.

(2) Comparing with strong wind, the sustained wind has larger fluctuating components at the Runyang Suspension Bridge site, which will induce stronger vibration response to the bridge. The fatigue stress under long-term wind load needs special consideration. The turbulence intensity at

the height of main girder is larger than that at the height of tower top, although the mean wind speed at this height is smaller. The turbulence intensity and gust factor have intensive correlation, so does the different components of the same parameter. Furthermore, the turbulence intensity increases proportionally with the gust factor ascending. With the airflow slowing down, the intensity of turbulence wind has the increasing tendency.

(3) As a parameter presents the scale of turbulence eddies, the turbulence integral length is larger than the value suggested by the design specifications of long-span bridge, which means this item defined in the bridge design specification can not suit for the practical condition of Runyang Suspension Bridge very well. For this region, it is suggested that the restriction of the long-span bridge design specification concerning the turbulence integral length should be ease at the height of main girder; but at height of tower top, it should be tightened. The turbulence integral length descends with the turbulence intensity increasing and ascends with the mean wind speed increasing.

(4) Both the Simiu spectrum employed by long span bridge design specification and Von Karman usually used for estimate the measurement fluctuating wind can not describe the wind energy distribution over frequency on the bridge site correctly. The parameters that utilized to describe power spectrum have close relationship with the mean wind speed, the distribution of those parameters has random characteristics. The appropriate power spectrum reflecting the fluctuating wind characteristics in this region needs further research.

(5) The wind field in mid-span has strong randomicity because of the influence of the earth surface roughness. The data recorded by the anemometer on tower top performs perfect regulations. Therefore, at difference height of one position, different wind models should be employed to describe the characteristics of fluctuating wind. The statistical results based on a large number of field measurement data are more reasonable.

Furthermore, the conclusions deduced in this paper are only based on the data of one year measurement at the Runyang Suspension Bridge site. More general conclusions should be obtained through wider field measurement data and further research. It is very necessary to add the database of field measurement wind not only strong wind but also sustained wind and execute comprehensive investigation through out of China.

Acknowledgments

The authors are grateful for the joint support of the National Natural Science Foundation of China (No. 51178100), Key Program of Ministry of Transport (No. 2011318223190), Natural Science Foundation of Jiangsu Province (No. BK2011141), Project of the Priority Academic Development Program of Jiangsu Higher Education Institutions (No. 1105007001), Teaching and Research Foundation for Excellent Young Teacher of Southeast University (No. 3205001205).

References

Andersen, O.J. and Lovseth, J. (1995), "Gale force maritime wind, the Froya data base. Part 1: sites and instrumentation, review of the database", *J. Wind Eng. Ind. Aerod.*, **57**(1), 97-109.

Brownjohn, J.M.W., Bocciolone, M., Curami, A., Falco, M. and Zasso, A. (1994), "Humber bridge full-scale measurement campaigns 1990-1991", *J. Wind Eng. Ind. Aerod.*, **52**(1-3), 185-218.

BWEA. UK Wind Speed Database[DB/OL] (2008), http://www. bwea. com/noabl/index.html
Ding, Y.L. and Li, A.Q. (2011), "Temperature-induced variations of measured modal frequencies of steel box girder for a long-span suspension bridge", *Int. J, Steel Struct.*, **11**(2), 145-155.
Flay, R.G.J. and Stevenson, D.C. (1998), "Integral length scales in strong winds below 20-m", *J. Wind Eng. Ind. Aerod.*, **28**(1-3), 21-30.
Li, Q.S., Dai, Y. M., Li, Z.N. and Hu, S.Y. (2010), "Surface layer wind field characteristics during a severe typhoon 'Hagupit' landfalling", *J. Build. Struct.*, **31**(4), 7-14. (in Chinese)
Kato, N., Ohukuma, T., Kim, J.R., Marukawa, H. and Niihori, Y. (1992), "Full scale measurements of wind velocity in 2 urban areas using an ultrasonic anemometer", *J. Wind Eng. Ind. Aerod*., **41**(1-3), 67-78.
Liu, T.T., Xu, Y.L., Zhang, W.S., Wong, K.Y., Zhou, H.J. and Chan, K.W.Y. (2009), "Buffeting-induced stresses in a long suspension bridge: structural health monitoring oriented stress analysis", *Wind Struct.*, **12**(6), 479-504.
Mann, J., Kristensen, L. and Courtney, M.S. (1991), *The great belt coherence experiment-a study of atmospheric turbulence over water*, Riso National Laboratory, Denmark.
Morfiadakis, E.E., Glinou, G.L. and Koulouvari, M.J. (1995), "The suitability of the von Karman spectrum for the structure of turbulence in a complex terrain wind farm", *J. Wind Eng. Ind. Aerod.*, **62**(2-3), 237-257.
Pakzad, S.N. (2010), "Development and deployment of large scale wireless sensor network on a long-span bridge", *Smart Struct. Syst.*, **6**(5-6), 525-543.
Panofsky, H.A. and Dutton, J.A. (1984), *Atmospheric turbulence-models and methods for engineering applications*, Wiley, New York.
Simiu, E. and Scanlan, R.H. (1996), *Wind effects on structures*. Wiley, New York.
Song, L.L., Pang J.B., Jiang C.L., Huang, H.H. and Qin, P. (2010), "Field measurement and analysis of turbulence coherence for Typhoon Nuri at Macao Friendship Bridge", *Sci. China: Technol. Sci.*, **53**(10), 2647–2657.
Sparks, P.R., Reid, G.T., Reid, W.D., Welsh, S. and Welsh, N. (1992), "Wind conditions in hurricane Hugo by measurement, inference, and experience", *J. Wind Eng. Ind. Aerod.*, **41**(1-3), 55-66.
Toriumia, R., Katsuchib, H. and Furuyac, N. (2000), "A study on spatial correlation of natural wind", *J. Wind Eng. Ind. Aerod.*, **87**(2-3), 203-216.
Wang, H., Li, A.Q., Guo, T. and Xie, J. (2009), "Field measurement on wind characteristic and buffeting response of the Runyang Suspension Bridge during typhoon Matsa", *Sci. China Series E: Technol. Sci.*, **52** (5), 1354-1362
Wang, H., Li, A.Q., Jiao, C.K. and Li, X.P. (2010), "Characteristics of strong winds at the Runyang Suspension Bridge based on field tests from 2005 to 2008", *J. Zhejiang Univ.-Sci. A*, **11**(7), 465-476.
Wu, Z.K., Zhao, L., Zhu, L.D. and Ge, Y.J. (2010), "High-altitude observation about turbulence characteristics for "Krosa" (0716) strong typhoon", *Acta Aerodynam. Sinica*, **28**(3), 291-296. (in Chinese)
Xiao, Y.Q., Li, L.X. and Song, L.L. (2009), "Study on typhoon wind characteristics based on field measurements", *Proceedings of the 7th Asia-Pacific Conference on Wind Engineering*, Taiwan.
Xu, Y.L. and Zhan, S. (2001), "Field measurements of Di Wang Tower during Typhoon York", *J. Wind Eng. Ind. Aerod.*, **89**(1), 73-93.
Xu, Y.L. and Zhu, L.D. (2005), "Buffeting response of long-span cable-supported bridges under skew winds. Part 2: Case study", *J. Sound Vib.*, **281**(3-5), 675-687
Xu, Y.L., Guo, W.W., Chen, J., Shum, K.M. and Xia, H. (2007), "Dynamic response of suspension bridge to typhoon and trains. I: Field measurement results", *J. Struct. Eng. - ASCE*, **133**(1), 3-11.
Zhang, X.J. (2011), "Investigation on the wind-induced instability of long-span suspension bridges with 3D cable system", *Wind Struct.*, **14**(3), 209-220
Zhao, L., Zhu, L.D. and Ge, Y.J. (2009), "Monte-Carlo simulation about typhoon extreme value wind characteristics in Shanghai region", *Acta Aerodynam. Sinica*, **27**(1), 25-31. (in Chinese)